American Society of Mechanical Engineers

ASME Accepted Manuscript Repository

Institutional Repository Cover Sheet

Cranfield Collection of E-Research - CERES

ASME Paper Title: Flow Distortion into the Core Engine for an Installed Variable Pitch Fan in Reverse Thrust Mode

Authors: David John Rajendran , Vassilios Pachidis

ASME Journal Title: Journal of Turbomachinery

Volume/Issue: _Volume 143, Issue 7____ Date of Publication (VOR* Online) 26 February 2021____

ASME Digital Collection URL: _https://asmedigitalcollection.asme.org/turbomachinery/article/doi/10.1115/1.4050331/1101292/Flow-Distortion-into-the-Core-Engine-for-an

DOI: https://doi.org/10.1115/1.4050331

*VOR (version of record)

Journal of Turbomachinery Received: September 21, 2020
Accepted manuscript posted: January 5, 2021
DOI:/10.1115/1.4050331
Copyright ©2021ASME

Journal of Turbomachinery, Volume 143, Issue 7,
Article number 071001,
Paper number TURBO-20-1252

FLOW DISTORTION INTO THE CORE ENGINE FOR AN INSTALLED VARIABLE PITCH FAN IN REVERSE THRUST MODE

David John Rajendran*

Rolls-Royce UTC, Centre for Propulsion Engineering,

Cranfield University,

Cranfield, Bedfordshire, MK43 0AL, UK

e-mail: d.rajendran@cranfield.ac.uk

Vassilios Pachidis

Rolls-Royce UTC, Centre for Propulsion Engineering,

Cranfield University,

Cranfield, Bedfordshire, MK43 0AL, UK

e-mail: v.pachidis@cranfield.ac.uk

ABSTRACT

The flow distortion at core engine entry for a Variable Pitch Fan (VPF) in reverse thrust mode is described from a realistic flow field obtained using an integrated airframe-engine model. The model includes the VPF, core entry splitter, complete bypass nozzle flow path wrapped in a nacelle and installed to an airframe in landing configuration through a pylon. A moving ground plane to mimic the rolling runway is included. 3D RANS solutions are generated at two combinations of VPF stagger angle and rotational speed settings for the entire aircraft landing run from 140 to 20 knots. The internal reverse thrust flow field is characterized by bypass nozzle lip separation, pylon wake and recirculation of flow turned back from the VPF. A portion of the reverse stream flow turns 180° with separation at the splitter leading edge to feed the core engine. The core engine feed flow exhibits circumferential and radial non-uniformities that depend on the reverse flow development at different landing speeds. The temporal dependence of the distorted flow features is also explored by an URANS analysis.

Total pressure and swirl angle distortion descriptors, as defined by the Society of Automotive Engineers (SAE) S-16 committee, and, total pressure loss into the core engine are described for the core feed flow at different operating conditions and landing speeds. It is observed that the radial intensity of total pressure distortion is critical to core engine operation, while the circumferential intensity is within acceptable limits. Therefore, the baseline sharp splitter edge is replaced by two larger rounded splitter edges of radii, ~0.1x and ~0.2x times the core duct height. This was found to reduce the radial intensity of total pressure distortion to acceptable levels. The

Published by The American Society of Mechanical Engineers. This is the Author Accepted Manuscript issued with:Creative Commons Attribution License (CC BY).
The final published version is available online at DOI: 10.1115/1.4050331. Please refer to any applicable publisher terms of use.

description of the installed core feed flow distortion, as described in this study, is necessary to ascertain stable core engine operation, which powers the VPF in reverse thrust mode.

Keywords: Variable Pitch Fan, reverse thrust, installed flow field, distortion, core engine operability.

INTRODUCTION

As the bypass ratio of future turbofan engines reach high values in the order of 10 – 14, the optimum fan pressure ratio to maximize propulsive efficiency reduces because of engine thermodynamic cycle considerations. The fan operability issues that may so develop in low pressure ratio fans can be managed by a VPF in which the fan stagger angle setting is varied. When the VPF aerofoils are rotated by 90° in the clockwise or anti-clockwise direction looking radially inward, the direction of airflow reverses because of the rearward shift in the cascade capture throat area. The rotation in the clockwise direction through feather pitch, places no restriction on the solidity, and is therefore preferred to the anti-clockwise rotation through flat pitch. The change in airflow direction with VPF stagger setting can be used to generate reverse thrust in an engine and eliminate the cascade based thrust reverser, which will be proportionally more bulky in future high bypass ratio engines because of the large fan diameter.

The feasibility of using VPF to generate reverse thrust was studied by NASA in the Quiet Clean Short-haul Experimental Engine (QCSEE) and the Advanced Ducted Propulsor (ADP) programs. In the QCSEE program, a reverse flow capable VPF engine with flared outlet nozzle petals was tested in an outdoor rig at static conditions and at limited forward flow conditions in a wind tunnel to demonstrate the levels of reverse thrust achievable. The ADP program focused on the development of a low noise reverse flow capable VPF design for future turbofan engines. Scaled down rig tests were done to characterize the reverse flow fan in an isolated static engine. The reverse flow fan aerodynamic behavior in the ADP test rig was described in a recent computational study [1-5]. All the previous studies explored the reverse flow behavior in uninstalled isolated static conditions or in limited forward flow conditions to characterize the reverse flow fan. The understanding of VPF in reverse thrust was extended in a recent study by the authors, by providing insight into the evolution of the actual installed reverse thrust fan flow field during the entire aircraft landing run from 140 knots to 20 knots, using an integrated airframe-engine model [6, 7].

However, besides the understanding of the reverse thrust fan flow field, an important aspect to be considered if the VPF is to be used for generating reverse thrust, is the satisfactory operation of the core engine for providing power to the VPF during reverse flow operation. The stable operation of the core engine in reverse thrust mode depends on the distortion levels and the total pressure loss of the core engine feed flow, which in turn depends on the reverse flow development within the engine internal flow path. In the previous NASA studies, except for limited total pressure, total temperature and static pressure surveys at different engine axial stations, no detailed information regarding the reverse flow development within the engine and the flow distortion transferred into the core engine was

obtained, even in the isolated uninstalled static conditions. In the computational ADP reverse flow study, the flow quality into the core engine was not described for the uninstalled rig condition. However, such information on details of flow at the core engine entry in reverse flow mode in the installed actual engine operating environment is crucial to successfully assess the suitability of the reverse thrust VPF as an aircraft thrust reversal system.

Therefore, the 3D RANS flow field obtained from an integrated airframe-engine research model for different aircraft landing speeds and VPF operational settings is used in this study to describe the installed internal reverse flow development and estimate the distortion and total pressure loss into the core engine. The influence of flow unsteadiness on the convection of distortion into the core engine is also explored from an URANS flow field to verify the transience of the distortion descriptors. Since the core engine operability is known to be influenced particularly by distortions in the total pressure and flow swirl, the corresponding distortion indices are computed for the different flow conditions. Minor design modifications that can be considered to alleviate undesirable distortion indices are also explored in the study.

INTEGRATED AIRFRAME-ENGINE MODEL

The integrated airframe-engine model is developed to study the VPF reverse thrust behavior in a typical modern 40000 lbf two-spool geared turbofan engine with 14 bypass ratio at design point and 110 inch fan inlet diameter. The VPF blade aerofoil design, which operates satisfactorily in both forward and reverse flow, is developed using the NASA ADP rig 22 inch diameter fan design as baseline. The VPF design used in this study has a forward flow pressure ratio of 1.27, temperature ratio of 1.08, hub to tip ratio of 0.3 and a tip speed of 245 m/s. The ability of the VPF design to induce suction and generate reverse flow is verified by a 3D RANS analysis of only the VPF in a duct. The VPF only reverse flow characterization is carried out for different fan rotational speeds and fan stagger angle settings. The study of the reverse flow characteristics revealed that: 1. Two stagger angle settings, ζ_1° and $\zeta_2^\circ = \zeta_1^\circ - 6^\circ$, indicate a wide operating range, with reverse flow pressure ratios in the range of 1.1 to 1.2, and reverse stream mass flows in the range 0.4x to 0.55x of design mass flow. 2. The bounds of reverse thrust behavior can be captured by exploring two fan rotational speeds, N_1 and $N_2 = 0.8N_1$. Both the stagger angle settings are within ±10° from the 90° through feather aerofoil rotation position, and the fan rotational speeds are within ±15% of the maximum fan rotational speed at the engine landing operational point. Therefore, the installed reverse thrust flow field exploration is carried out at different combinations of the VPF stagger angle and rotational speed settings for the entire aircraft landing run from 140 knots to 20 knots.

The VPF in the engine is installed to a representative twin-engine airframe with high lift devices and spoilers set in landing configuration. The model includes a full annular representation of engine internal flow path: VPF stage with 18 aerofoils, core engine splitter, core entry duct, bypass nozzle duct, 40 Outlet Guide Vane (OGV) blade row aerofoils, core nozzle exhaust duct, aft-body casing

and plug. The engine model is wrapped in a representative modern nacelle geometry and attached to the airframe through a bespoke pylon design at a typical wing chord location finalized from an installation aerodynamics study. A moving ground plane is defined as the base of a large far-field domain within which the integrated airframe-engine model is placed, to mimic the rolling runway. Figure 1 shows the different components of the integrated airframe-engine model. The computational grid for the integrated model is generated using a hybrid domain discretization strategy that uses a combination of unstructured and structured elements based on the sub-domain flow. A total grid size of ~73 million elements is finalized for the model after an extensive grid sensitivity study of different local and global flow parameters with maximum Grid Convergence Index (GCI) for any parameter not exceeding 0.006 in any sub-domain.

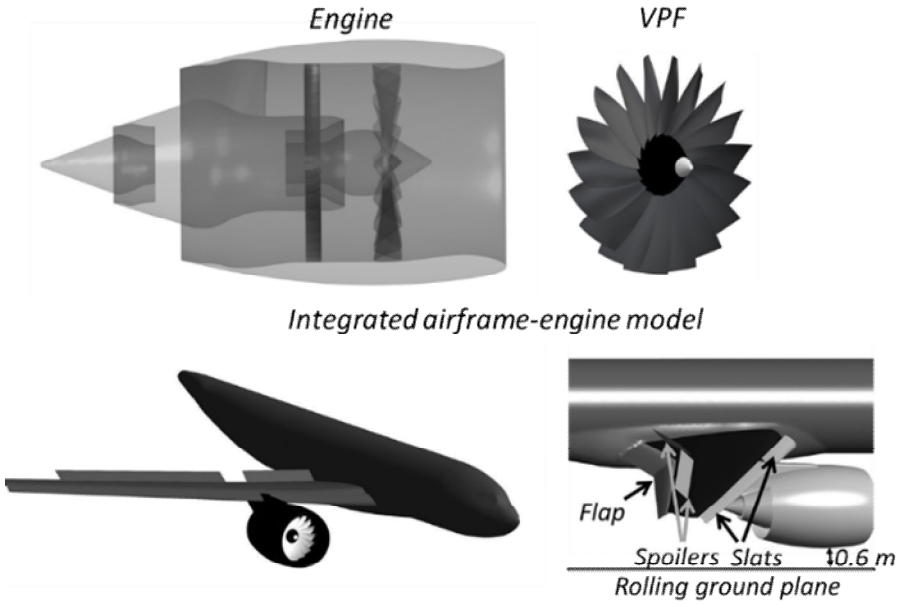


FIGURE 1: COMPONENTS OF INTEGRATED AIRFRAME-ENGINE MODEL [6]

A 3D RANS solution of the reverse thrust flow field is generated from a finite volume code, ANSYS-CFX that solves the RANS equations using a conservative fully implicit second order resolution algorithm. The turbulence closure is specified by the two equation k-ω Shear Stress Transport (SST) model and the near-wall flow physics is explicitly resolved. The flow field vector solution space is generated by specifying as boundary conditions: the far-field free stream velocity and ground plane velocity which correspond to the aircraft landing speed, at each VPF stagger angle – rotational speed combination. The development of the reverse flow into the core engine is generated as part of the flow field solution. The boundary condition to mimic the core engine entry is specified in terms of axial velocity, equivalent to a mass flow distribution, at the core entry plane, as obtained from the engine performance model for the chosen fan rotational speed engine operating point. The choice of the core engine thermodynamic state as a boundary condition does not impose a specific back pressure that would influence the core engine flow development, but instead preserves the distortion in terms

of the flow properties transferred into the core engine from the reverse stream development within the bypass duct. The computational solutions are obtained with physical advection timescales that vary depending on the flow timescales in different sub-domains. Statistical measures of convergence that compare the standard deviations of different parameters of interest over fixed iteration intervals are defined to determine the stopping convergence criteria, specified as <0.5% variation over iteration bands. Further details about the individual component module development, domain discretization and flow field solution schematics of the integrated airframe-engine model to obtain the reverse thrust flow field are discussed in the publications dealing with the fan flow field and model development [6, 7].

DISTORTION DESCRIPTORS

The stable operation of the core engine compressor is known to be primarily affected by flow distortions that occur because of non-uniformity in total pressure and swirl angle. The effect of flow distortion on compressor performance has been studied by using descriptors to quantify the extent of flow distortion. Of the number of descriptors available in the literature to quantify distortion, the industry standard Society of Automotive Engineers (SAE) S-16 committee definition of descriptors for the total pressure distortion and swirl distortion are chosen to quantify the flow distortion at the core compressor entry plane. This is because a particular value of the S-16 committee descriptors can be interpreted to ascertain the operability of a range of compressor designs [8, 9]. To compute S-16 committee flow descriptors, the annular plane at which the indices are to be quantified, is discretized by using a standard 8-rake 5-ring measurement point definition as shown in Figure 2. The rings divide the annulus into equal areas and the rakes are placed at equal 45° intervals. The outermost ring near the shroud is designated ‘1’ and a right hand polar co-ordinate system with the first quadrant in the top right corner is used for the angle definition.

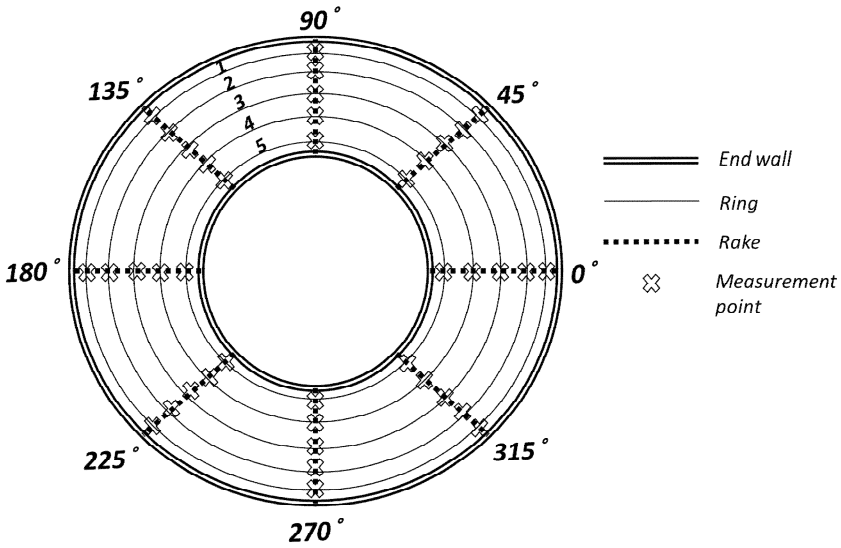


FIGURE 2: 8 RAKE 5 RING CONVENTION

Total Pressure Distortion Indices

The total pressure distortion is defined using four descriptors – three of which relate to the circumferential non-uniformity and is calculated for each ring, and, one to define the radial non-uniformity computed for the annular face. The circumferential non-uniformity quantifiers of the total pressure distortion, for each ring, are:

1. Extent: Angular sector below the ring average defined as

$$\theta_i = \theta_{2,i} - \theta_{1,i} \tag{1}$$

Where θ is the circumferential extent for ring i. Subscripts 1 and 2, indicate the angular location at which the ring average total pressure intersects the total pressure distribution at different circumferential locations.

2. Circumferential Intensity: Average circumferential total pressure depression in each identified extent ($PAVLOW_i$) as compared to the ring average (PAV_i) expressed as Circumferential Distortion Index (CDI_i).

$$PAV_i = \frac{1}{360}\int_0^{360} P(\theta)_i d\theta \tag{2}$$

$$PAVLOW_i = \frac{1}{\theta_j}\int_0^{\theta_j} P(\theta)_i d\theta \tag{3}$$

$$CDI_i = \frac{PAV_i - PAVLOW_i}{PAV_i} \tag{4}$$

Where $P(\theta)$ is the total pressure distribution in a ring. In the case of multiple extents the maximum CDI for the ring computed from the minimum depressed total pressure average value is presented in this study.

3. Multiple-Per-Revolution (MPR): number of extents with average total pressure lower than ring average total pressure.

The radial non-uniformity quantifier for the face is defined as:

4. Radial Intensity: Minimum ring average total pressure ($PAV_{i,\,min}$) as compared to the face average total pressure ($PFAV$) expressed as Radial Distortion Index (RDI).

$$RDI = \frac{PFAV - PAV_{i,min}}{PFAV} \tag{5}$$

The effect of total pressure distortion on the core engine operation is felt as a reduction in the compressor surge pressure ratio. The reduction in the surge pressure ratio depends on the sensitivity factors of the compressor to circumferential and radial distortion indices. A preliminary guideline of CDI and RDI threshold values to define a safe limit for stable compressor operation can be estimated from the reported loss in surge pressure ratio for compressors responding to a number of standard circumferential and radial distorted inlet flows. With the consideration that a loss in surge pressure ratio of <5% would be a typical acceptable limit for safe operation, the threshold CDI and RDI values are estimated as 0.07 [10-18].

In this study, the defined threshold values are used as a preliminary guide to understand the severity of the total pressure distortion indices. The reported realistic reverse flow total pressure distortion indices can then be used in studying the response of any compressor design using separate extensive distortion response experimental or computational analysis. Moreover, the reverse flow distortion indices can also provide information to design compressors, which are tolerant to such distortions that may be critical to engine operation with the VPF in reverse thrust mode.

Swirl Angle Distortion Indices

The swirl angle distortion indices are defined to characterize the type of the swirl flow field at an annular plane. The different types of swirl flow field are shown in Figure 3. For any generic swirl flow field, three indices are defined to characterize the distribution of swirl angle in each ring:

1. Swirl intensity: Average of the absolute swirl angle, independent of direction. It is calculated by separately computing the sector swirl for each sector of positive swirl and negative swirl in the face.
2. Swirl directivity: Direction equivalent of bulk swirl for a ring. It is calculated as a ratio of the summation of sector swirl areas with the direction included to the summation of absolute sector swirl areas. The value ranges from -1 to 1, with -1 for negative bulk swirl, +1 for positive bulk swirl, 0 for twin swirl, value > 0 for positive offset swirl and value < 0 for negative offset swirl.
3. Swirl pair: Number of swirl angle direction changes in a ring. The value is computed as a ratio of the summation of the absolute sector swirl areas to the maximum sector swirl. Swirl pair along with swirl directivity is used to compute regions of alternating flow direction in a swirl flow field. The values range from 0.5 to 1, with 0.5 indicating no direction change in positive/negative bulk swirls, 1 indicating symmetric direction change in twin swirl and values in the range 0.5 to 1 indicating the extent of asymmetry in direction change for positive/negative offset swirl.

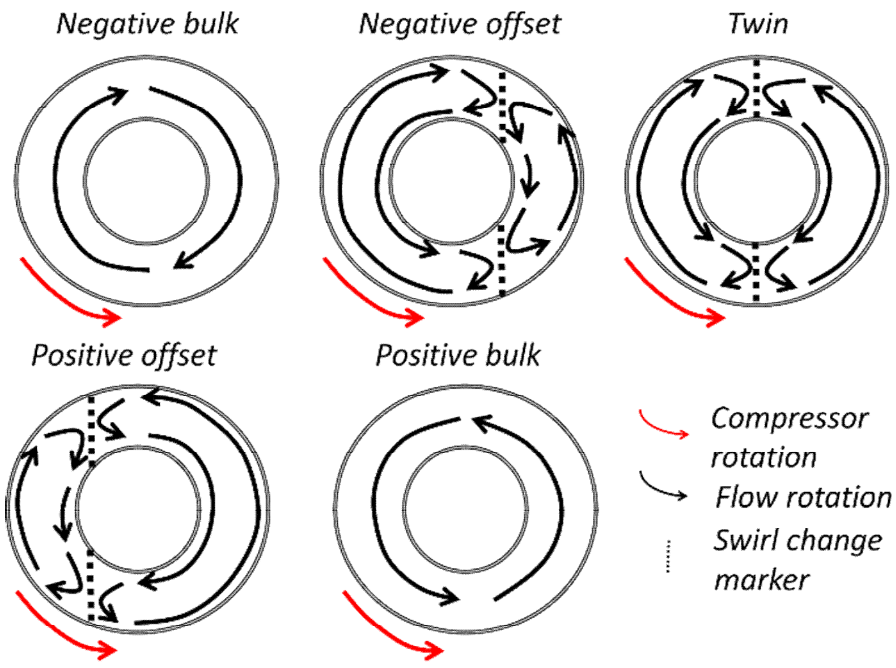


FIGURE 3: GENERAL TYPES OF SWIRL FLOW FIELD

The effect of swirl distortion on the compressor operability depends on the type of the swirl flow field. The swirl flow field influences the flow incidence at the compressor inlet plane and the effect of this blade row incidence is felt as a change in the mass flow handling capacity of the compressors. Therefore, in this study for the reverse flow at core engine entry, the swirl flow field type is identified from the swirl distortion indices, and the swirl angle distribution is presented to aid in the calculation of compressor blade row incidence. The identification of swirl flow field and swirl angle distribution can be used to understand the severity of the incidence that might be expected at the compressor blade row entry and suitably design the blade row for optimal forward and reverse flow performance.

RESULTS AND DISCUSSIONS

In this study to describe the flow distortion in the core engine feed flow, the results are discussed in the following manner:

1. A brief description of general installed reverse thrust flow field to provide an appreciation of the VPF reverse thrust flow field and act as a context for the distortion study. The development of the installed reverse thrust flow field and the evolution of fan flow field during the landing run for different operating conditions are discussed in detail in [6, 7].
2. Total pressure and swirl angle distortion at 110 knots landing speed for the VPF at ζ_I°-N_I setting. To understand the distortion at the core engine entry for the 110 knots case, a detailed discussion on the reverse flow development within the engine internal flow path from the bypass nozzle exit is included.

3. Effect of landing speed on the distortion indices for the VPF at ζ_1°-N_1 setting.
4. Effect of the change in VPF operational setting on the distortion indices for all landing speeds.
5. A note on the transience of distortion indices obtained from URANS analysis at 110 knots.
6. Total pressure loss into the core engine for all landing speeds including the effect of change in VPF operational settings.

After the description of the reverse flow core engine distortion is completed, a design modification study to manage undesirable distortion behavior is described.

General Installed Reverse Thrust Flow Field

The general reverse thrust flow field at 110 knots landing speed for the VPF at ζ_1°-N_1 operating point is shown using external and internal projected flow streamline sketches at the mid-engine surface in Figure 4. When the VPF is engaged in reverse thrust mode during the aircraft landing run, the flow is ingested from the bypass nozzle exit and ejected out of the fan inlet with an imparted swirl component due to fan rotation. The free stream penetrates into the fan from the nacelle inlet in the central inner annular regions and is entrained to join the reverse stream that occupies the outer annular regions. As the reverse stream reaches the nacelle lip, it is washed down at an angle towards the engine exit region by the free stream. The washed down flow, as it reaches the engine exit regions and comes under the influence of fan suction, turns 180° into the engine at the bypass nozzle exit, thereby leaving a separation at the bypass nozzle lip.

After the reverse stream enters the engine at the bypass nozzle exit, it continues developing towards the fan, through the OGV passages in the bypass duct. Thereafter, at the splitter, one portion of the reverse stream turns 180° to enter the core engine, while leaving a separation at the splitter edge. The remaining portion enters the fan aerofoil passages, where it meets the free stream from the nacelle inlet in a shear layer. Within the fan passages, the reverse stream and entrained free stream flows are centrifuged radially outwards, and a part of it establishes the reverse flow out of the fan near the outer annulus. Because of the shear-layer interaction within the fan passages, another part of the centrifuged reverse stream flow turns back at the outer shroud towards the bypass nozzle exit. The turned back reverse stream, on which the fan work has been done, flows through the OGV, where it loses its momentum, and re-joins the reverse stream from the bypass nozzle exit. Further details about the general reverse thrust flow field and the evolution of the fan flow field at different landing speeds and operating conditions are discussed in [6, 7].

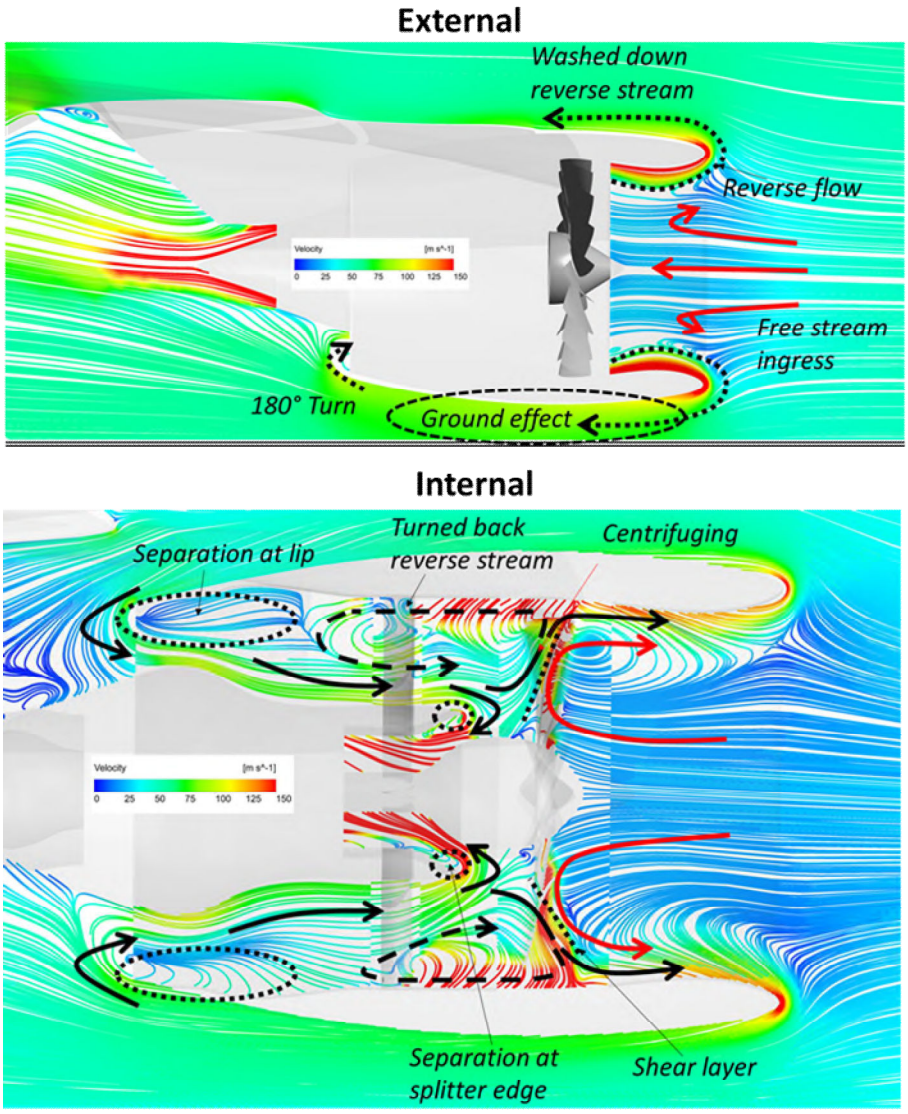


FIGURE 4: GENERAL REVERSE THRUST FLOW FIELD STREAMLINES

Distortion at 110 knots for ζ_1°-N_1 VPF

The reverse flow development from the bypass duct to the core engine entry at 110 knots landing speed is shown in terms of axial velocity and swirl angle contours in Figures 5 and 6 respectively. In Figure 5, the axial velocity is chosen to distinguish the reverse flow and forward flow at different stations. In Figure 6, the reverse flow in the bypass duct and into the core engine is clipped to show the swirl angle evolution within the engine.

At the bypass nozzle exit, there is a circumferential non-uniformity in the amount of reverse flow entering the engine. This is because at the engine exit region, the pylon blockage and the swirl in the washed down reverse stream from the nacelle lip result in a circumferentially varying flow field on which the fan suction acts. As the reverse stream develops in the bypass duct, circumferential

non-uniformity is added because of the pylon wake and differing amounts of interaction with the 'turned back reverse stream' from the fan. The reverse stream then passes through the OGV aerofoils and further circumferential non-uniformity due to blade row wake signature is added to it. A portion of this reverse stream flow turns into the core engine with the circumferential non-uniformity convected from the engine external regions, pylon wake, interaction with the 'turned back reverse stream' and passage through the OGV blade row.

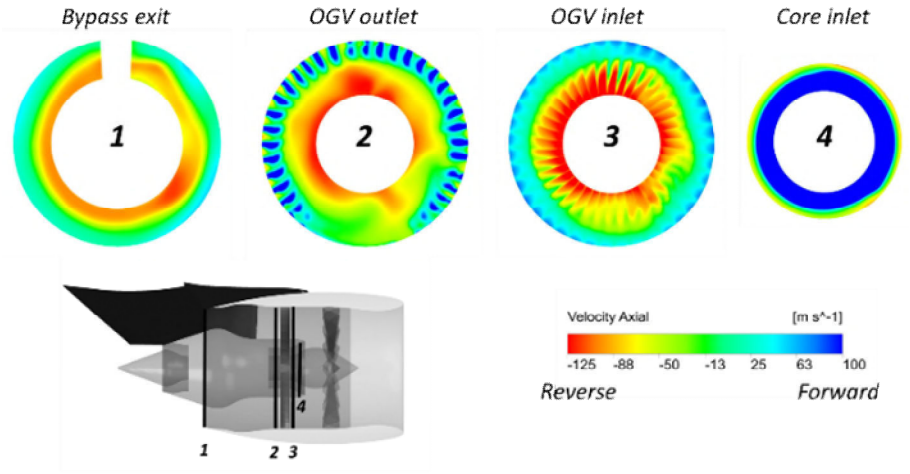


FIGURE 5: AXIAL VELOCITY CONTOURS AT DIFFERENT ENGINE STATIONS

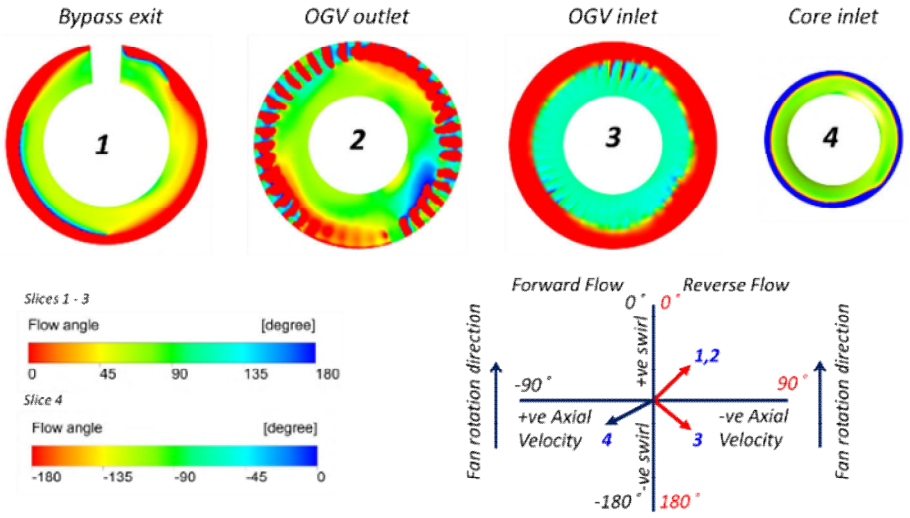


FIGURE 6: SWIRL ANGLE CONTOURS AT DIFFERENT ENGINE STATIONS

In addition to the circumferential non-uniformity, there is a radial non-uniformity at the bypass exit plane because of the nozzle lip separation. As the reverse flow develops in the bypass duct, additional radial non-uniformity is observed in the OGV inlet and outlet planes because of the interaction with the 'turned back reverse stream' from the fan. However, since it is the inner annular portion of the reverse stream that turns 180° into the core engine, the radial non-uniformities that lie in the outer annular regions in the bypass duct

are not convected into the core engine. Instead, the separation at the splitter edge because of the reverse flow turn to feed the core engine becomes the cause of the radial non-uniformity in the core feed flow.

The convection of the circumferential non-uniformity is influenced by the evolution of the reverse stream flow angle within the engine. The reverse flow enters the engine with 45°-70° angle because of the swirl in the washed down reverse stream flow from which it develops. As it develops in the bypass duct, further variation in the circumferential swirl angle distribution is introduced because of the pylon wake and re-joining of the 'turned back reverse stream'. However, after the bypass duct, since the reverse flow passes through the OGV blade row, the swirl angle variation reduces, and most of the reverse stream flow is deflected to values near the OGV inlet blade angle. The inner annular portion of the reverse stream flow at the OGV inlet angle turns to constitute the core feed flow. The inlaid vector sketch of Figure 6 shows the change in the bulk direction of the reverse stream as it develops within the engine stations. The reverse stream passage through the OGV before turning into the core engine tends to even out the large circumferential swirl variations of the reverse stream development in the bypass duct. However, minor residual swirl variations remain even after the passage through the OGV, and additional variations because of the flow wake mixing and the separation at the splitter edge are introduced in the core engine feed flow. The consequence of the circumferential and radial uniformities in the core feed flow, because of the reverse flow development within the engine, in terms of the flow distortion indices is discussed below.

Total Pressure Distortion Indices*:* The development of the flow distortion at the core engine entry plane in the vicinity of the splitter edge is shown in Figure 7 using the total pressure contours. The core engine entry plane is typically considered to be located after the reduction in the radius through the splitter.

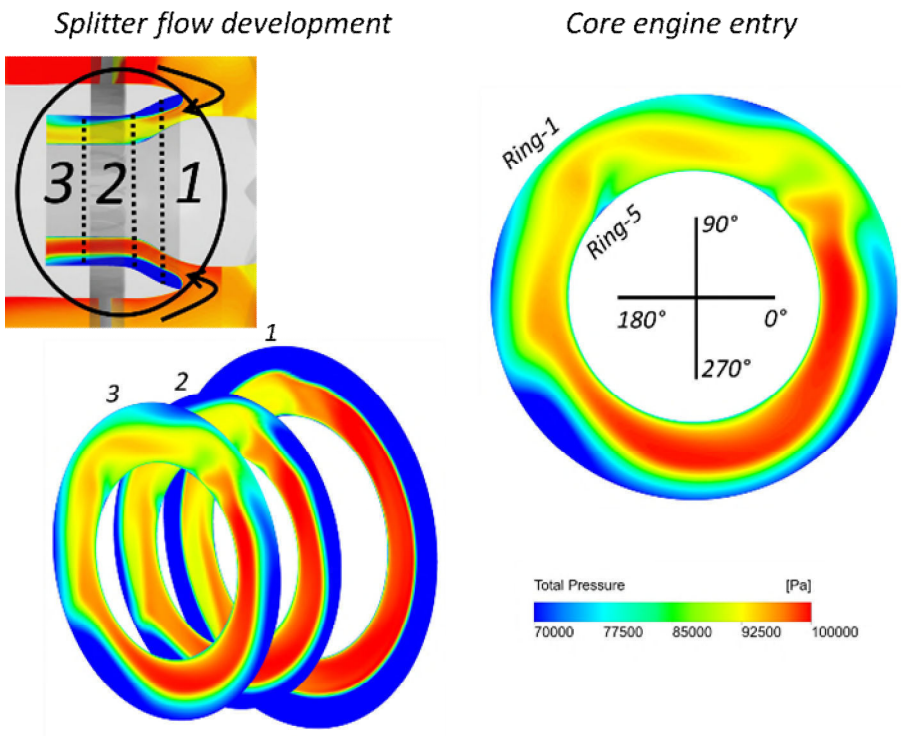


FIGURE 7: TOTAL PRESSURE CONTOURS AT CORE ENGINE ENTRY PLANE

The development of the flow non-uniformity at the core engine entry plane, after the 180° turn at the splitter edge, is influenced by the reduction in radius through the splitter duct geometry into the core engine. Three features characterize the total pressure distortion at the core entry: 1. the radial distribution of total pressure variation around the annulus because of the change in the extents occupied by the splitter edge separation, as the reverse flow develops through the splitter duct. 2. A total pressure depression in the angular sector 45° to 135° because of the pylon introduced flow non-uniformity. 3. Minor lobe like non-uniformities, at ~50° and ~120° locations, associated with flow separation in the core engine entry duct inner wall, after the splitter declension. The circumferential total pressure distortion indices at the core entry plane for each ring are shown in Figure 8. The computation of the RDI is shown in Figure 9.

As observed from the flow contours, the circumferential distortion indices indicate that in each ring the total extent of the depressed total pressure region varies from 130° to 180°. The depressed regions in Rings 2 to 4, indicate two MPR regions, corresponding to the pylon obstruction region divided by the inner wall separation. The computed CDI value for the bulk of core feed flow is below the acceptable value of 0.07, except for Ring 2. An anomalous higher value is observed in Ring 2 because of the location of a measurement point in the shear layer between the separated flow region and the bulk reverse flow. The computed RDI value of 0.117 is above the acceptable value of 0.07. The higher RDI value would leave the core engine susceptible to the occurrence of instabilities in reverse thrust mode operation.

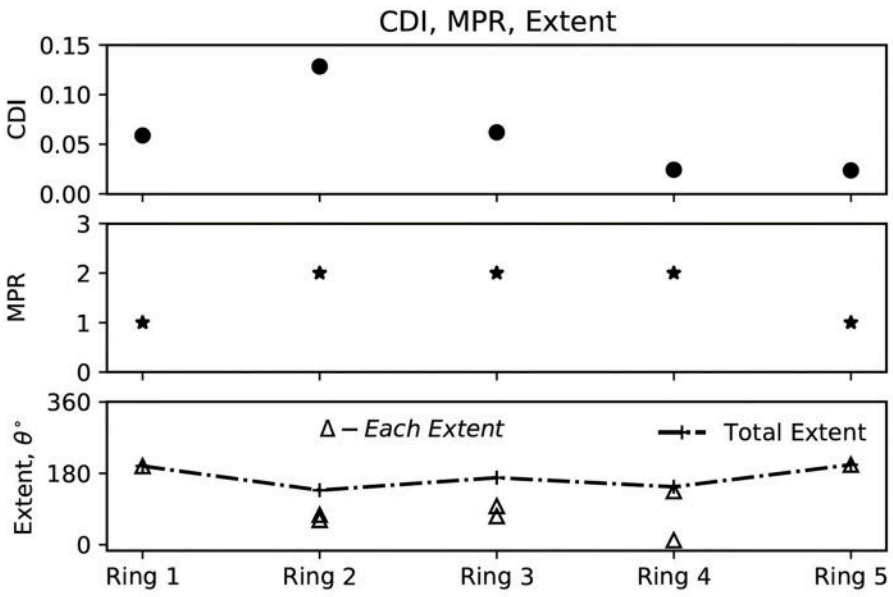


FIGURE 8: CIRCUMFERENTIAL TOTAL PRESSURE DISTORTION INDICES

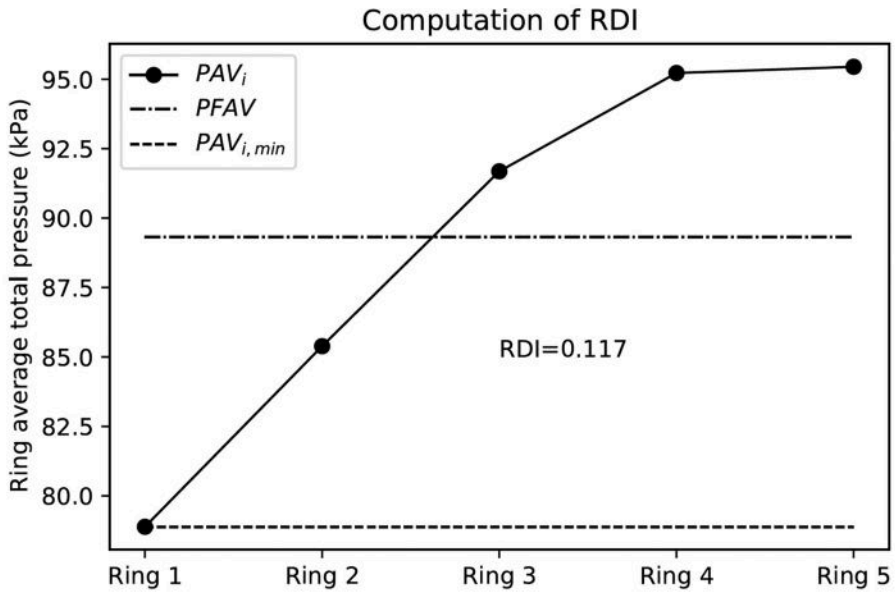


FIGURE 9: COMPUTATION OF RADIAL TOTAL PRESSURE DISTORTION INDEX

Swirl Angle Distortion Indices: Typically, an Engine Section Stator (ESS) row, is located in the splitter radius reduction region, and the core engine feed flow needs to develop through this aerofoil row to reach the core engine entry plane. Therefore, the swirl angle distortion indices are calculated at a plane that is ahead of the entry to the ESS, located upstream of Plane 1 in Figure 7. This plane is considered because after the passage through the ESS, the core feed flow would be deflected along the ESS outlet metal angle. As noted from the reverse flow direction sketch in Figure 6, the core feed flow is in the quadrant 3 ranging from -90° to -180°. For aiding ease of

interpretation and avoiding large negative numbers, a local 0° to 90° angle convention to represent the quadrant 3 is used to discuss the swirl angle distribution. The circumferential distribution of swirl angle in the local co-ordinate axes at the ESS entry plane is shown in Figure 10.

The flow contours and distribution indicate that the angle distribution of the core feed flow is determined by the OGV inlet metal angle, which varies from 24° at the hub to 26° at the tip, in the local co-ordinate axes. Deviation, wake mixing and the separation at the splitter edge results in a reduction of the core feed flow angle to an average of ~15° from the OGV metal angle. The pylon obstruction and the annular differences in the reverse stream properties result in circumferential variation of the angle distribution. The swirl distribution, without any change in the flow direction around the annulus, indicates that core feed flow is of the 'negative bulk swirl' type, with the flow pointing opposite to the direction of rotation. The computed swirl intensity values range from 13° to 15° for Rings 3 to 5, which are in the bulk core feed flow. Rings 1 and 2 located in the splitter edge separation region indicate random minor variations that are characteristic of separated flow. Since there are no annular changes from the negative swirl direction, the corresponding swirl directivity and swirl pair index are -1 and 0.5, respectively.

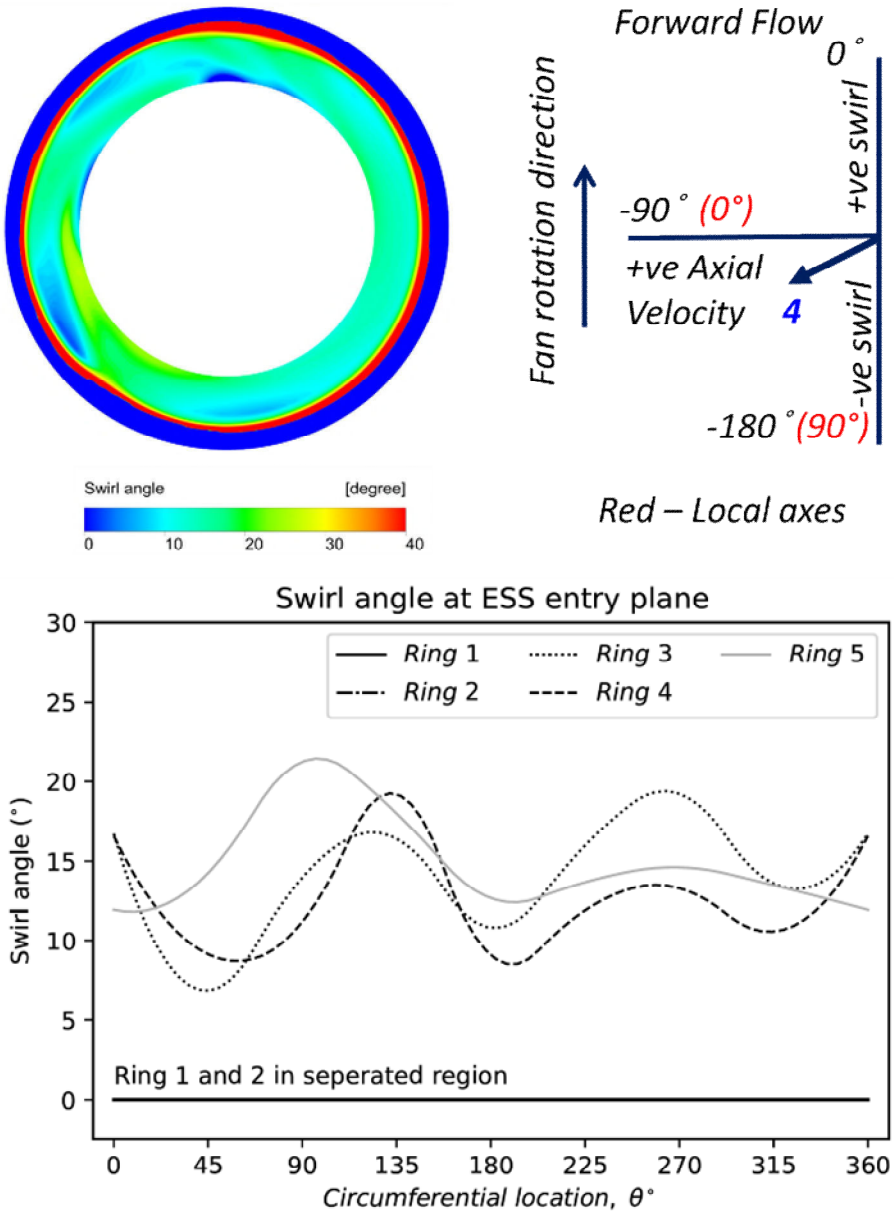


FIGURE 10: SWIRL ANGLE DISTRIBUTION INTO CORE ENGINE

The effect of the swirl angle distribution influences the flow incidence at the ESS blade row. To explore this, a representative ESS design to match the engine dimensions is developed from the ESS aerofoil geometry of the NASA ADP configuration, from which the OGV and the VPF used in this work are also developed. The ESS blade row is then placed in the splitter declension of the integrated airframe engine model and the reverse thrust flow field is generated. The overall flow field remains similar except for local changes after the flow passage through the ESS. The ESS design in the integrated model and the corresponding flow development into the core

engine entry plane at the 110 knots landing speed is shown in Figure 11. It is observed that the effect of the ESS is felt as a reduction in the average total pressure because of the loss associated with flow passage separation.

The ESS blade row developed from the NASA ADP design has a constant blade inlet metal angle of 6.5° along the span. Therefore, the reverse flow swirl distribution at the ESS entry plane results in a blade row incidence in the range of 2° to 13° for different blades around the annulus. The ESS design has high solidity (>2.5) and features rounded aerofoil section leading edges that can tolerate such incidence angles, as evidenced from the blade to blade mean section contour plot in Figure 11. However, even with such high solidities flow separation is observed near the trailing edge regions that result in an increase of the total pressure loss across the passages. It is to be noted that the ADP ESS design is different from the conventional ESS designs that feature sharp leading edge radii and tend to be cambered to de-swirl the flow. In such conventional ESS designs, the same reverse flow swirl angle distribution would result in large incidence values that would cause massive flow separation on the aerofoil pressure side. Therefore, it is recommended that particular attention needs to be paid to the flow turning and camber of the ESS row and the compressor inlet guide vane stator row, located before the first rotor, for satisfactory operation in both forward and reverse flow.

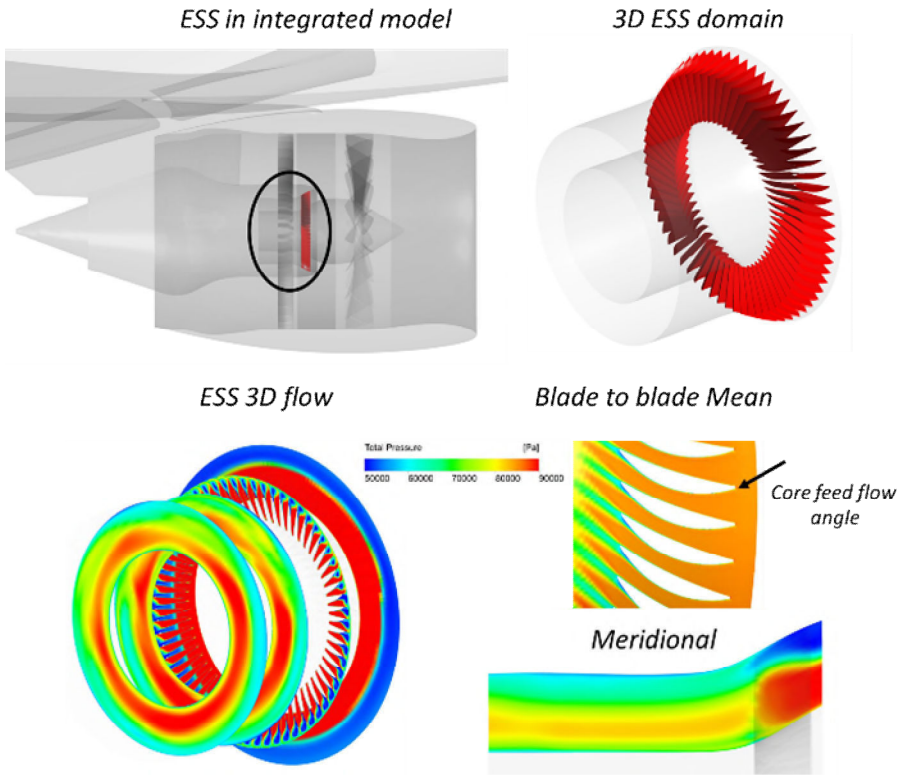


FIGURE 11: CORE FEED FLOW DEVELOPMENT THROUGH THE ESS

Further, the total pressure contour pattern at the core engine entry downstream of the ESS, Plane 3 in Figure 7, is similar to the case without the ESS, because the same pattern of flow distortion in the reverse stream is passed through the ESS blade row. A minor reduction in the splitter declension inner wall separation is observed because of the ESS flow guidance. Consequently, the computed CDI value is marginally lower for the case with the ESS. However, the RDI value with the ESS is similar to the case without the ESS because of the similar extent of splitter edge separation. Therefore, a conservative approach in which the total pressure distortion is considered without the alleviating effect on the CDI imposed by the ESS aerofoil guidance is adopted in this to study, to allow sufficient margin for safe compressor operation.

Effect of Landing Speed on Distortion for ζ_1°-N_1 VPF

As the aircraft landing speed decreases, there is an increase in the amount of reverse stream flow entering the engine because of the larger availability of slower moving free stream air at the engine exit regions which come under the influence of fan suction. The increase in the reverse stream flow and its subsequent development within the engine is shown using axial velocity contours in Figure 12 for three different landing speeds, 140 knots, 80 knots and 20 knots, corresponding to the beginning, middle and end of the aircraft landing run. Typically, the thrust reversers are shut-off at about 50 knots to prevent foreign object ingestion; the 20 knots case is yet considered to show the effect of landing speed for the entire landing run. The increase in the amount of reverse stream skews the momentum balance between the reverse stream and free stream in the fan aerofoil passages and reduces the amount of turned back reverse stream into the engine from the fan nominal outlet. This is observed as a reduction in the OGV wake signatures of the turned back reverse stream at the outer shroud regions in the OGV outlet plane. Additionally, the increased reverse stream at the lower landing speeds, fills out the annular flow passage circumferentially, as can be observed from the inner shroud regions at the OGV inlet plane; at higher speeds the reverse stream regions are interspersed with large wakes associated with a lower reverse stream mass flow, while in the lower speeds the wakes are well-defined thin regions associated with the OGV passage being filled with larger amount of reverse stream. Consequently, at lower speeds, the core feed flow develops from the 180° splitter turn of a larger momentum, more circumferentially uniform reverse stream.

The total pressure CDI and RDI values at all landing speeds are shown in Figure 13. The better circumferential uniformity is felt as a reduction in the total pressure CDI values with the reduction in landing speed. The progressive clustering of the individual ring CDI values to lower values is indicative of the improvement in the circumferential non-uniformity. The CDI values for the bulk core feed flow at all landing speeds are below the acceptable threshold of 0.07, except for few anomalous higher values observed primarily in Rings 1 and 2 where the measurement points are in the separated flow-bulk flow shear layer.

On the other hand, the larger momentum of the flow turning into the core engine with the reduction in landing speed, results in a larger separation at the splitter outer edge. Consequently, the larger radial portion occupied by the separated flow in the outer annular

regions of the core entry plane results in an increasing radial stratification of total pressure, which causes an increase in the RDI values with landing speed as shown in Figure 13.

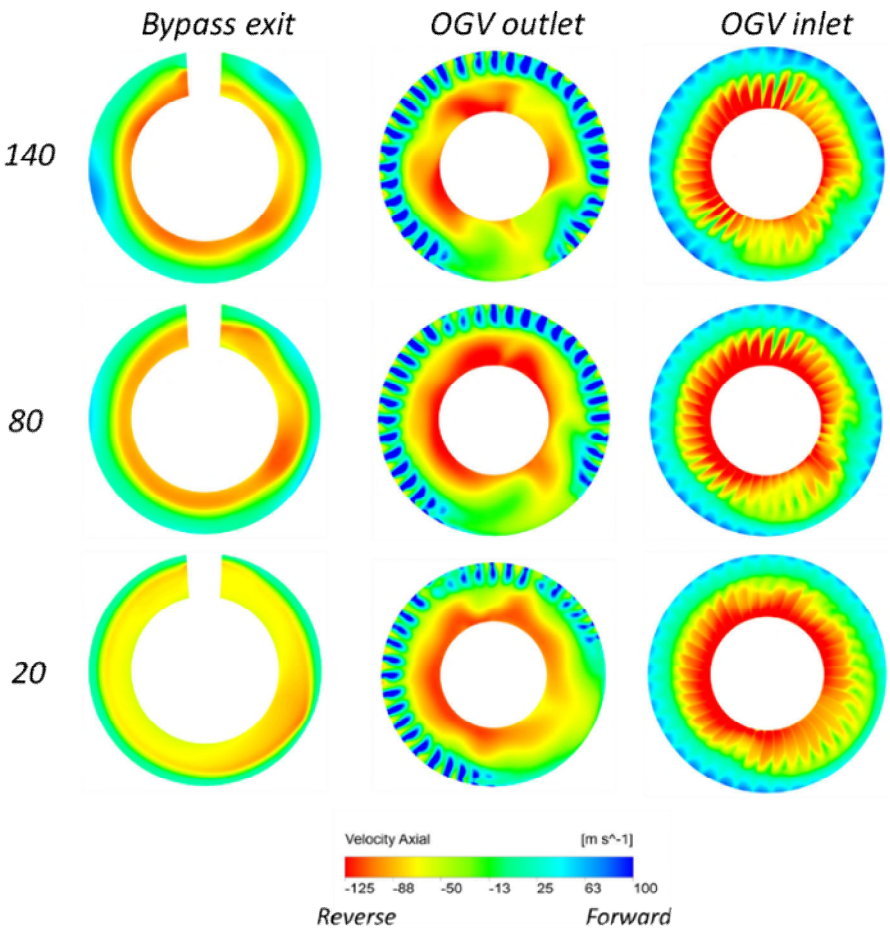


FIGURE 12: AXIAL VELOCITY CONTOURS AT DIFFERENT LANDING SPEEDS

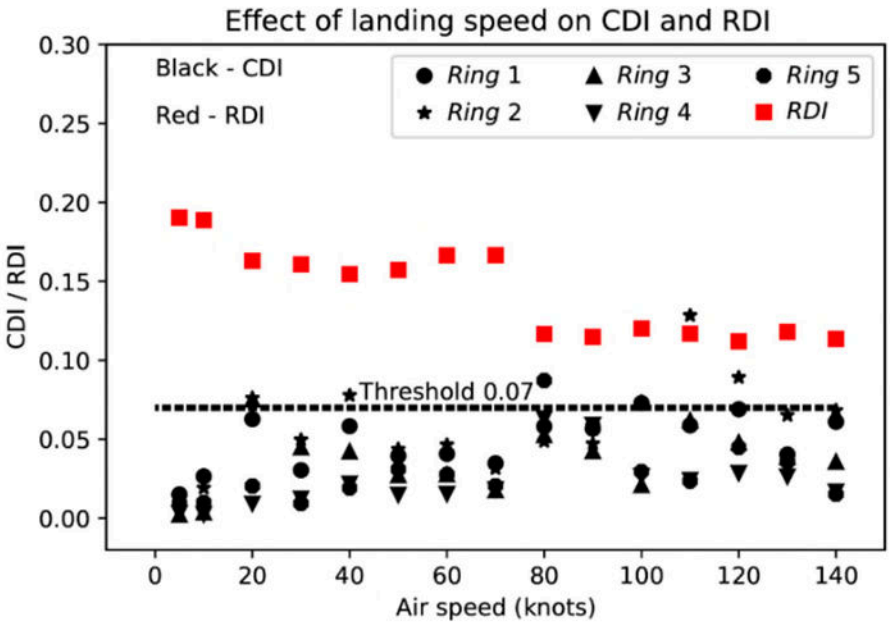


FIGURE 13: CDI AND RDI FOR DIFFERENT LANDING SPEEDS

At speeds below 80 knots, the larger outer annular regions occupied by the splitter edge separation forces the bulk of the core feed flow towards the inner annular region, which suppresses the separation in the core entry duct inner wall. The separation in the core inner duct, as shown in Figure 7, causes an upward deflection of the reverse stream into the core engine and reduces the separated region at the core entry plane. The reduction in the helpful inner wall separation further accentuates the effect of the splitter edge separation zone to be felt down into the core entry plane as a well-defined radial total pressure stratification. This change in the inner wall separation is observed as a discontinuity in the increase of RDI at 80 knots. The RDI values are above the acceptable threshold of 0.07 at all landing speeds.

The swirl angle distribution is not significantly affected by the landing speed because the reverse stream is deflected to the OGV inlet metal angle in all cases. Therefore, at all landing speeds, the swirl flow field type remains as 'negative bulk swirl' with an average swirl intensity of ~15°, swirl directivity of -1 and swirl pair index of 0.5.

Effect of VPF Setting on Distortion

The effect of VPF setting on distortion is discussed by considering: i) the change in fan rotational speed from N_1 to $N_2=0.8N_1$ at the ζ_1° stagger angle setting, and ii) the change in stagger angle setting from ζ_1° to $\zeta_2^\circ = \zeta_1^\circ - 6^\circ$ at the N_1 fan rotational speed, for all landing speeds. As the fan rotational speed is reduced, the effect of fan suction on the external flow field at the engine exit region is weaker, and consequently lower amount of reverse stream enters into the engine at the bypass nozzle exit. The total pressure CDI values and RDI values at all landing speeds for both the rotational speeds are shown in Figure 14. In the lower rotational speed as well, the reverse flow

develops through a similar internal flow field and convects circumferential non-uniformities due to the same reasons in to the core engine. Therefore, no significant changes are observed in the total pressure CDI values. However, since in the lower rotational speed, the momentum of the reverse stream turning into the core engine is lower, the extent occupied by the separation at the splitter edge is also lower. This results in the core feed flow to occupy proportionally larger regions of the inner annulus and reduce the radial stratification of total pressure, which is observed as a reduction in the total pressure RDI values.

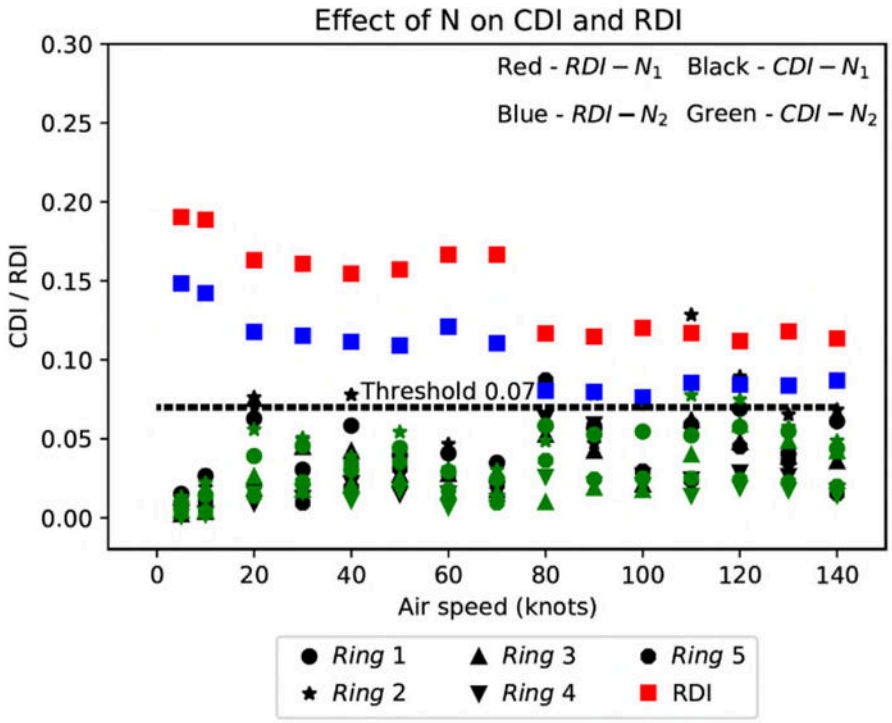


FIGURE 14: CDI AND RDI AT DIFFERENT FAN N FOR ALL LANDING SPEEDS

The reduction of the fan stagger angle causes the fan aerofoil passages to be more open from both the nominal inlet and outlet plane of the fan aerofoil cascade. Therefore, the marginally larger amount of reverse stream ingested from the bypass nozzle exit faces a larger blockage from the free stream that ingresses into the fan aerofoil passages from the more open inlet plane. This results in a larger proportion of the reverse flow to be turned back from the fan passages which interacts with reverse stream developing in the bypass duct. However, the minor re-distribution of internal flow field features with stagger angle does not significantly affect the properties of the core feed flow. Thus, the total pressure CDI and RDI values are in same range for both the stagger angle settings. Therefore, it is noted that irrespective of the fan operational setting, the total pressure CDI values are not critical while the RDI values are above the acceptable threshold for stable core engine operation.

The swirl angle distribution at the core entry plane does not exhibit significant variations with either the change in fan rotational speed or the fan stagger angle setting because of the development of the core feed flow through the OGV passages in all cases. Only minor changes, < 3° in swirl intensity, due to the change in the relative strength of the reverse flow OGV wake because of the differing reverse stream momentum in the different cases is observed.

Note on Transience of Distortion Indices

URANS analysis of the integrated airframe-engine model is carried out at the 110 knots aircraft landing speed to explore the temporal dependence of the core feed flow distortion indices. The transient term is discretized using a second order backward Euler scheme which is robust, implicit and conservative in time. The time step is defined in such a way that each complete rotation of the VPF is captured in 100 discrete time steps. The independence of the solution to the time step selection is verified by evaluating the solution at three different time step choices viz. half, double and a non-harmonic fraction of the chosen time step. Each time step requires ~41 minutes of CPU time in a 128 core 16 parallel Message Passing Interface (MPI) process setup in the in-house High Performance Computing (HPC) facility 'DELTA' with a peak processing speed of 60 Teraflops. 3000 time steps are required to reach the periodicity stopping criteria, which makes the total computational time for the URANS analysis to be ~2000 hours.

The core feed flow total pressure and swirl angle distortion indices are computed for all the time steps in three fan rotations, which equal nearly twelve core compressor rotations. The evolution of the transient total pressure distortion indices are driven by the convection timescale (~0.6 millisecond) of the circumferential non-uniformities from the bypass nozzle exit into the splitter edge and the core engine entry plane. Another faster time scale (~0.04 millisecond) is also observed for the convection of the splitter declension inner wall separation to the core engine entry plane. Minor fluctuations are observed in the extent of separation at the splitter edge corresponding to the periodic convection of the pylon wake obstruction and circumferential variation in the distribution of the reverse stream flow momentum. Per-rev (per 1 compressor rotation) average and per-rev peak filters are applied to the distortion indices computed at each time step to verify whether the distorted flow patterns computed from the steady state analysis are retained over a complete revolution of the core compressor. Both the per-rev average and per-rev peak filtered distortion values indicate that the total pressure CDI and RDI values are within ±2% of the steady state values. No change is observed in the swirl angle distribution because of the similar flow deflection at all time steps. Therefore, since the flow distortion pattern at the core engine entry plane is because of the pylon wake, splitter inner wall separation and the separation at the splitter edge, all of which are not time dependent flow features, the observations regarding the criticality of total pressure RDI values are also verified from the unsteady flow field.

Pressure Loss into Core Engine

The absolute value of total pressure at the core engine entry plane depends on the reverse stream total pressure loss as it develops through the engine internal flow path into the core engine. A feature of the internal reverse thrust flow field aids the core engine entry total pressure in the reverse flow mode to have reasonable values near the forward flow mode value. This beneficial effect is because of the interaction of the turned back flow from the fan outlet, which is at a higher total pressure because of fan work addition, with the reverse stream developing from the bypass exit, which pressurizes the reverse stream flow. The pressure loss of the reverse stream, computed as a difference between the average total pressure at the bypass nozzle exit and the average total pressure at the core entry plane, normalized with the ambient pressure, for different aircraft landing speeds and VPF operational settings is shown in Figure 15. The reverse stream has a near ~10% pressure loss as it develops within the engine. The main sources of the loss are the pylon wake, OGV wakes, and splitter edge separation. The reverse stream pressure loss is independent of the aircraft landing speed, because the effect of increased reverse stream momentum with landing speed is offset by the circumferential filling of the reverse stream flow, which reduces the extent occupied by the separated wake regions. The lower rotational speed indicates a lower pressure loss because of the reduction in the extent of the splitter edge separation due to the lower reverse stream mass flow. The stagger angle setting of the fan does not affect the reverse stream pressure loss.

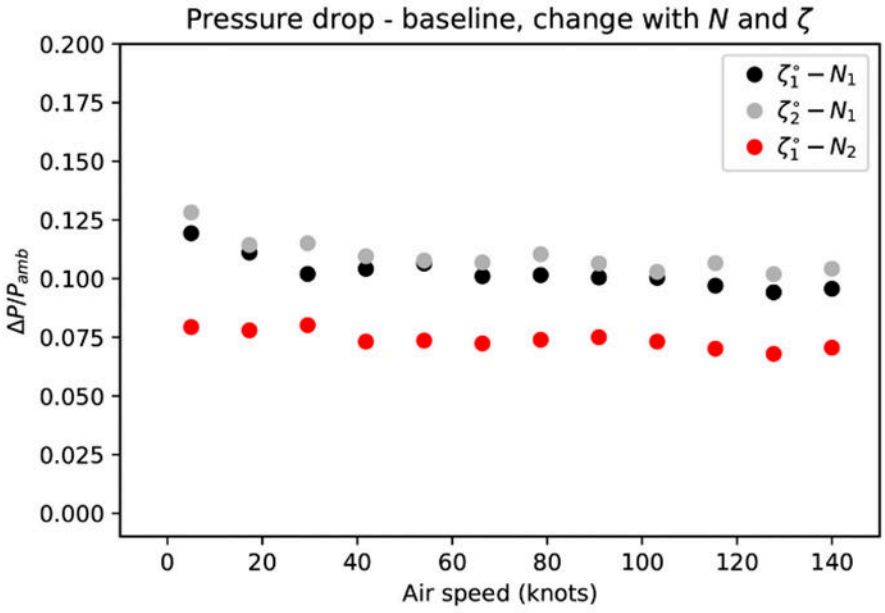


FIGURE 15: REVERSE STREAM PRESSURE LOSS FOR DIFFERENT VPF SETTINGS

The average total pressure at the core entry plane in reverse thrust mode is ~0.9P_{amb} (ambient pressure at sea-level) for the ζ_1°-N_1 VPF setting, as compared to the ~1.1P_{amb} in the nominal forward flow condition; fan forward flow pressure ratio near the hub regions is 1.1. The difference in the core entry total pressure is ~0.2 P_{amb} between the reverse mode and forward flow mode. This difference

reduces to ~0.1 P_{amb} for the more benign ζ_1°-N_2 VPF setting. The reverse mode-forward mode total pressure difference is higher at the outer annular regions because of the splitter edge separation, while in the bulk core feed flow the difference is minimal. The extent of the radial skew in the total pressure difference is captured in the RDI values, and if the RDI values are reduced below the acceptable threshold of 0.07, the absolute total pressure at the core engine entry can also be brought near the forward flow values.

Splitter Edge Design Modification Study

In order to reduce the unacceptable total pressure RDI values, which arises because of the size and extent of the splitter edge separation, a design parametric study on the splitter edge radius is explored. The baseline splitter edge with 2 mm reverse flow turn radius is replaced by rounded splitter edges of 20 mm, ~0.1x core duct height, (~golf ball) and, 40 mm, ~0.2x core duct height (~tennis ball) turn radii, as shown in Figure 16. The rounding of the splitter edge is done by trimming the length to accommodate the spherical surface and thus preserve the flow path definition in the bypass duct and into the core engine. The effect of the increase in splitter edge radius on nominal forward flow is tested by a 3D RANS solution of the splitter domains for the cruise operating condition. The fan outlet flow profiles in terms of total pressure, total temperature and flow angle are specified as the inlet boundary, and the mass flux into the core engine and bypass nozzle is specified at the two outlet boundaries. The splitter total pressure loss is computed by adding the total pressure losses in the core flow and the bypass flow. It was observed that the splitter total pressure loss was not significantly affected by the radii increase. This is because, even though the total pressure deficit in the larger radii are higher, the deficit occurs over shorter lengths. Additionally, in order to preclude any minor back pressure related influences of the larger splitter radii on fan forward flow operation, the larger splitter radii can alternatively be implemented in the engine along with a detached sharp edge island splitter located axially ahead of the rounded regions.

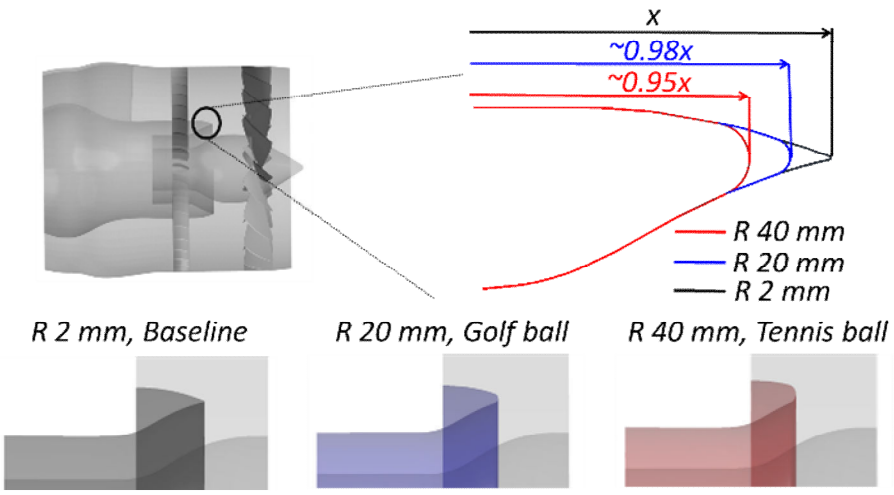


FIGURE 16: SPLITTER EDGE DESIGN PARAMETRIC STUDY

The reverse flow behavior obtained from the integrated airframe-engine at an aircraft landing speed of 110 knots and VPF at ζ_1°-N_1 setting for the three different splitter radii in the vicinity of the splitter is shown in Figure 17. The smooth flow turn passage through the rounded splitter radii results in a reduction and extent of the separation zone at the splitter edge. The total pressure RDI values and total pressure loss into the core engine for all the three splitters at all landing speeds are shown in Figure 18 and Figure 19 respectively.

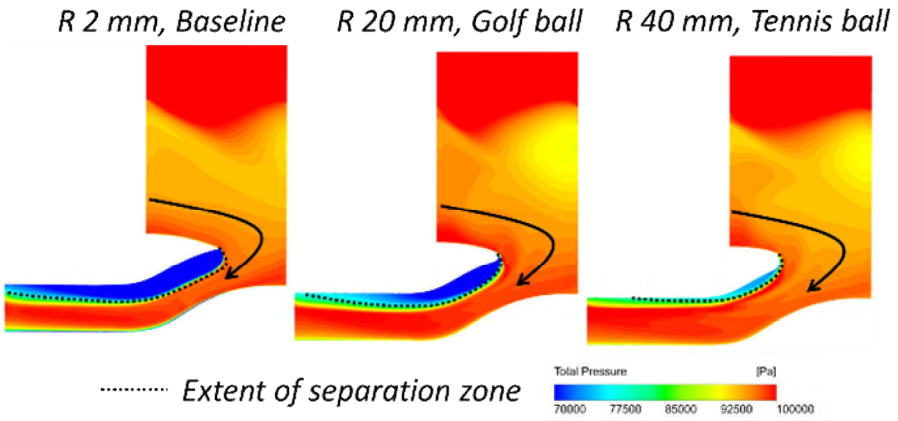


FIGURE 17: REDUCTION IN EDGE SEPARATION WITH INCREASE IN RADII

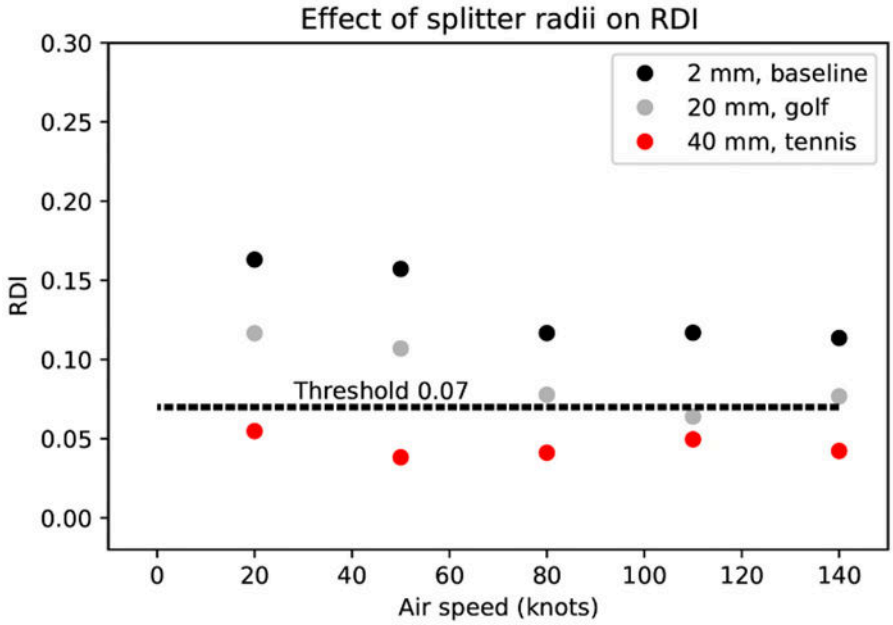


FIGURE 18: RDI VALUES FOR DIFFERENT SPLITTER RADII

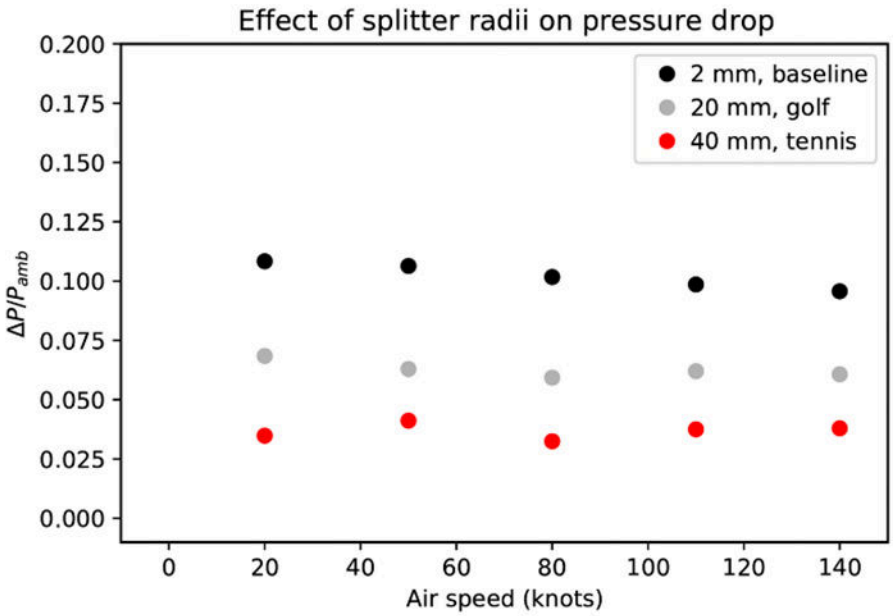


FIGURE 19: REVERSE STREAM PRESSURE LOSS FOR DIFFERENT SPLITTER RADII

It is observed that in the typical landing speed range of thrust reverser engagement, 140 knots to 60 knots, the golf ball sized splitter is barely above the acceptable threshold value of 0.07. In the tennis ball sized splitter, the RDI levels are below the acceptable threshold for all aircraft landing speeds from 140 knots to 20 knots. The reduction of the RDI values are also observed as an increase in the absolute total pressure at the core engine entry, nearer to the forward flow values, as indicated by the reduction in the reverse stream total pressure loss. The total pressure CDI values, the swirl angle distribution, and the general revere thrust flow field are similar for all the three splitter radii. Therefore, it is recommended that at least a golf ball sized splitter turn radius for the reverse flow entry into the core engine is required for satisfactory core engine operation in reverse thrust mode.

CONCLUSIONS

An integrated airframe-engine model is used to describe the flow distortion into the core engine during the reverse thrust mode operation of the VPF at different operational settings during the entire landing run of the aircraft. The details of the core engine flow quality in terms of total pressure and swirl angle distortion indices, as obtained from a realistic representation of the installed VPF reverse thrust flow field, are necessary to ascertain the ability of the core engine to operate satisfactorily during the aircraft landing run and provide power to rotate the VPF engaged in reverse thrust mode. The key observations and recommendations from this study are:

1. The development of the reverse flow within the internal engine flow path from the bypass nozzle exit into the core engine is provided to describe the non-uniformities that manifest as distorted flow at the core engine entry plane. Since an integrated full annular model is used, a true representation of flow non-uniformities, both external and internal to the engine, is captured.
2. Description of the total pressure circumferential and radial non-uniformity in terms of CDI and RDI values along with the identification of flow features responsible for the development of total pressure distortion. It is observed that the CDI values are within an acceptable range while the RDI values are critical to core engine operation for the baseline geometry examined.
3. The evolution of swirl within the engine internal flow path and into the core engine is described in detail. It is observed that the flow at the core entry is a 'negative bulk' type swirl flow field. The ability of a representative ESS design to work satisfactorily in such a swirl flow field is demonstrated. It is emphasized that particular care needs to be taken in optimizing the flow turning in the ESS blade row and the first stator of the core engine for satisfactory forward and reverse flow operation.
4. A splitter edge design modification study has indicated that the RDI values can be reduced to acceptable levels by rounding the splitter edge radius to at least ~0.1x core duct height. The limited impact of such rounding of the radius in forward flow operation has been verified by analysis in cruise operating conditions.

The description of the distortion in the core engine entry plane with the realistic reverse thrust flow field features can provide direction for suitable design development studies in the future to reduce the distortion levels and to minimize the impact of distortion on core engine operation. Different engine architectures and design modifications to reduce non-uniformities and flow distortion into the core engine are currently being explored. Additionally, the response of a representative core engine compressor stage while operating with the flow distortion obtained in this study is planned to be explored.

ACKNOWLEDGMENTS

The authors would like to express their gratitude to Rolls-Royce plc. for supporting this research and for permission to publish the paper. Special thanks to Mr. Richard Tunstall, Mr. John Whurr and Mr. Barry Moore of Rolls-Royce plc. for comments and suggestions.

NOMENCLATURE

Abbreviations

ADP	Advanced Ducted Propulsor
CDI	Circumferential Distortion Index
ESS	Engine Section Stator
GCI	Grid Convergence Index

MPR	Multiple Per Revolution
OGV	Outlet Guide Vane
QCSEE	Quiet Clean Short-haul Experimental Engine
RANS	Reynolds-Averaged Navier Stokes
RDI	Radial Distortion Index
SAE	Society of Automotive Engineers
SST	Shear Stress Transport
URANS	Unsteady Reynolds-Averaged Navier Stokes
VPF	Variable Pitch Fan

Symbols

N	rotational speed
C	combined distortion constant
k	turbulence kinetic energy
P	total pressure
PAV	average total pressure
PAVLOW	Depressed sector average total pressure
PFAV	Face average total pressure
α	swirl angle
ζ	stagger angle
θ	extent angle
ω	specific dissipation rate

Subscripts

amb	Ambient
i	ring
j	extent counter

REFERENCES

[1] Samanich, N.E., Reemsnyder, D.C. and Bloomer, H.E., 1980. “Reverse thrust performance of the QCSEE variable pitch turbofan engine”. SAE Transactions, 89, pp.3623-3650, available at www.jstor.org/stable/44632622

[2] Schaefer, J.W., Sagerser, D.R. and Stakolich, E.G., 1977. “Dynamics of high-bypass-engine thrust reversal using a variable-pitch fan”. NASA, Washington, DC, Report No. NASA TM X-3524.

[3] Hobbs, D.E., Neubert, R.J., Malmborg, E.W., Philbrick, D.H. and Spear, D.A., 1995. “Low Noise Research Fan Stage Design”. NASA, Washington, DC, Report No. NASA-CR-195382.

[4] Tweedt, D.L., 2014. “Computational aerodynamic simulations of an 840 ft/sec tip speed advanced ducted propulsor fan system model for acoustic methods assessment and development”. NASA, Washington, DC, Report No. NASA/CR-2014-218129.

[5] Williams, T. S., and Hall, C. A., 2019. “Reverse Thrust Aerodynamics of Variable Pitch Fans”. *ASME.* J. Turbomach, 141(8): 081008. https://doi.org/10.1115/1.4043139

[6] Rajendran, D. J., and Pachidis, V., 2019. "Fan Flow Field in an Installed Variable Pitch Fan Operating in Reverse Thrust for a Range of Aircraft Landing Speeds." ASME. J. Eng. Gas Turbines Power. October 2019; 141(10): 101018. https://doi.org/10.1115/1.4044686

[7] Rajendran, D.J., Bentley, D., Aguirre, H.A., Tunstall, R., and Pachidis, V., 2020. “Development of a Research Model to Study the Operability of a Variable Pitch Fan Aero Engine in Reverse Thrust.”. In Global Power & Propulsion Society Chania 2020 Proceedings, GPPS, Chania. https://doi.org/10.33737/gpps20-tc-43

[8] SAE S-16 Technical Committee, 1978. “Gas Turbine Engine Inlet Flow Distortion Guidelines”. ARP 1420b, Society of Automotive Engineers, inc.

[9] SAE S-16 Technical Committee, 1983. “Inlet Total-Pressure Distortion Considerations for Gas Turbine Engines”. SAE. Report-*AIR1419*.

[10] Davis Jr, M.W., Hale, A.A. and Klepper, J., 2010. “40 Years of AEDC Development, Evolution and Application of Numerical Simulations for Integrated Test and Evaluation of Turbine Engine Turbomachinery Operability Issues”. Aerospace Testing Alliance, Arnold AFB TN, No. AEDC-TR-09-T-19.

[11] Beale, D., Davis, M. and Sirbaugh, J., 2006 . “Requirements and advances in simulating aircraft inlet total pressure distortion in turbine engine ground tests”. ASME Paper No. GT2006-90038

[12] Davis, Jr, M., 1991. “Parametric investigation into the combined effects of pressure and temperature distortion on compression system stability”. AIAA Paper No. AIAA-91-1895-CP

[13] Hercock, R.G. and Williams, D.D., 1974. “Distortion-induced engine instability aerodynamic response”. AGARD, LS72-Paper, 3.

[14] Milner, E.J., 1977. “Analytical Prediction of the Performance and Stability of a J85-13 Compressor with distorted Inlet Flow”. NASA, Washington, DC, Report No. NASA-TM-X-3515.

[15] Hah, C., Rabe, D.C., Sullivan, T.J. and Wadia, A.R., 1998. “Effects of inlet distortion on the flow field in a transonic compressor rotor”. *ASME.* J. Turbomach, 120(2), pp.233-246.

[16] Soeder, R.H. and Mehalic, C.M., 1984. “Effect of combined pressure and temperature distortion orientation on high-bypass-ratio turbofan engine stability”. NASA, Washington, DC, Report No. NASA TM 83771.

[17] Cousins, W.T. and Davis, M.W., 2011, January. “Evaluating complex inlet distortion with a parallel compressor model: Part 1—Concepts, theory, extensions, and limitations”. ASME Paper No. GT2011-45067

[18] Davis, M.W. and Cousins, W.T., 2011, January. “Evaluating complex inlet distortion with a parallel compressor model: Part 2—Applications to complex patterns”. ASME Paper No. GT2011-45068



https://dspace.org/

Flow distortion into the core engine for an installed variable pitch fan in reverse thrust mode

Rajendran, David John; Pachidis, Vassilios

2021-02-26
ASME
https://doi.org/10.1115/1.4050331
Rajendran DJ, Pachidis V. (2021) Flow distortion into the core engine for an installed variable pitch fan in reverse thrust mode. Journal of Turbomachinery, Volume 143, Issue 7, Article number 071001, Paper number TURBO-20-1252

Downloaded from a DSpace repository. https://dspace.org/